Iterative expansion microscopy

Jae-Byum Chang[1,2], Fei Chen[3], Young-Gyu Yoon[1,4], Erica E Jung[1], Hazen Babcock[5], Jeong Seuk Kang[6], Shoh Asano[1], Ho-Jun Suk[7], Nikita Pak[8], Paul W Tillberg[4], Asmamaw T Wassie[3], Dawen Cai[9] & Edward S Boyden[1,3,10,11]

We recently developed a method called expansion microscopy, in which preserved biological specimens are physically magnified by embedding them in a densely crosslinked polyelectrolyte gel, anchoring key labels or biomolecules to the gel, mechanically homogenizing the specimen, and then swelling the gel–specimen composite by ~4.5× in linear dimension. Here we describe iterative expansion microscopy (iExM), in which a sample is expanded ~20×. After preliminary expansion a second swellable polymer mesh is formed in the space newly opened up by the first expansion, and the sample is expanded again. iExM expands biological specimens ~4.5 × 4.5, or ~20×, and enables ~25-nm-resolution imaging of cells and tissues on conventional microscopes. We used iExM to visualize synaptic proteins, as well as the detailed architecture of dendritic spines, in mouse brain circuitry.

© 2017 Nature America, Inc., part of Springer Nature. All rights reserved.

We recently discovered that preserved biological specimens that are embedded in a swellable polymer gel with key biomolecules or labels anchored to the gel and then mechanically homogenized could be isotropically swelled ~4.5× in linear dimension by immersion in water—a process we call expansion microscopy (ExM)[1]. Since our original paper on ExM, we have developed variants that anchor proteins or RNA directly to the gel, enabling application to diverse scientific and clinical contexts[2,3]. However, all ExM variants published to date expand biological specimens by ~4.5× in linear dimension, resulting in an effective resolution for an ~300-nm diffraction-limited objective lens of ~60–70 nm (~300/4.5), which led us to ask the question of whether expansion factors greater than ~4.5× might be possible, which in turn could lead to still better resolution.

In our original ExM protocol[1], biological molecules of interest were first labeled with a primary antibody and then by a secondary antibody bearing an oligonucleotide. Then, a second oligonucleotide bearing a gel-anchoring moiety (a 5′ acrydite group) and a fluorophore was applied and anchored to a swellable polyelectrolyte gel synthesized evenly throughout the specimen. After mechanical homogenization with strong protease treatment, the polymer–specimen composite could then be expanded in water[1]. Expanding a gel >4.5-fold was possible[1] but resulted in fragile gels. We here explored whether it would be possible to synthesize, postexpansion, a second gel that could expand the specimen further and still provide sufficient mechanical support (**Fig. 1a**–**e**). To develop such an iterative ExM (iExM) protocol, we had to transfer the information (i.e., the anchored fluorophores, antibodies, or biomolecules) from the first gel to the second, disrupt the first gel, and expand the second gel.

RESULTS

Design of iterative expansion microscopy chemistry

We implemented iExM by first taking a sample and expanding it using ExM as in our original paper[1], but we applied the second oligonucleotide (green in **Fig. 1f**) without a fluorophore and used a cleavable crosslinker (e.g., the commercially available crosslinker N,N′-(1,2-dihydroxyethylene) bisacrylamide (DHEBA), whose diol bond can be cleaved at high pH[4]) for gel synthesis (**Fig. 1g**). We then embedded the expanded sample in an uncharged polyacrylamide gel prepared with a cleavable crosslinker (the re-embedding gel[3]) so that the sample could be held in the expanded state during subsequent steps. Importantly, this re-embedding gel allowed us to apply a third oligonucleotide (**Fig. 1h**), bearing a gel-anchoring moiety and fluorophore, which hybridized to the oligonucleotide anchored to the first polymer. We then formed a second polyacrylate gel, made with a conventional crosslinker (e.g., N,N′-methylenebis(acrylamide) (BIS)), which incorporated the third oligonucleotide (and thus the fluorophore, **Fig. 1i**), and then we dissolved the original gels by cleaving their crosslinkers before expanding the fluorophores away from each other through immersion in water (**Fig. 1j**). iExM typically resulted in expansion ratios of ~4.5–5.5× in the first round and ~4× in the second round for a total increase of ~16–22× (see **Supplementary Note 1** for details). In addition to this implementation of iExM, we explored using the re-embedding gel as the final gel and hydrolyzing the side groups at high pH into carboxyl groups[5] (dissolving the first gel's crosslinkers simultaneously), a process we call 'high pH' iExM (hp-iExM). hp-iExM resulted in

[1]Media Lab, Massachusetts Institute of Technology (MIT), Cambridge, Massachusetts, USA. [2]Department of Biomedical Engineering, Sungkyunkwan University, Suwon, Korea. [3]Department of Biological Engineering, MIT, Cambridge, Massachusetts, USA. [4]Department of Electrical Engineering and Computer Science, MIT, Cambridge, Massachusetts, USA. [5]Harvard Center for Advanced Imaging, Harvard University, Cambridge, Massachusetts, USA. [6]John A. Paulson School of Engineering and Applied Sciences, Harvard University, Cambridge, Massachusetts, USA. [7]Harvard-MIT Division of Health Sciences and Technology, MIT, Cambridge, Massachusetts, USA. [8]Department of Mechanical Engineering, MIT, Cambridge, Massachusetts, USA. [9]Department of Cell and Developmental Biology, Medical School, Biophysics Research Division, LS&A, University of Michigan, Ann Arbor, Michigan, USA. [10]McGovern Institute, MIT, Cambridge, Massachusetts, USA. [11]Department of Brain and Cognitive Sciences, MIT, Cambridge, Massachusetts, USA. Correspondence should be addressed to E.S.B. (esb@media.mit.edu).

RECEIVED 4 SEPTEMBER 2016; ACCEPTED 20 MARCH 2017; PUBLISHED ONLINE 17 APRIL 2017; DOI:10.1038/NMETH.4261

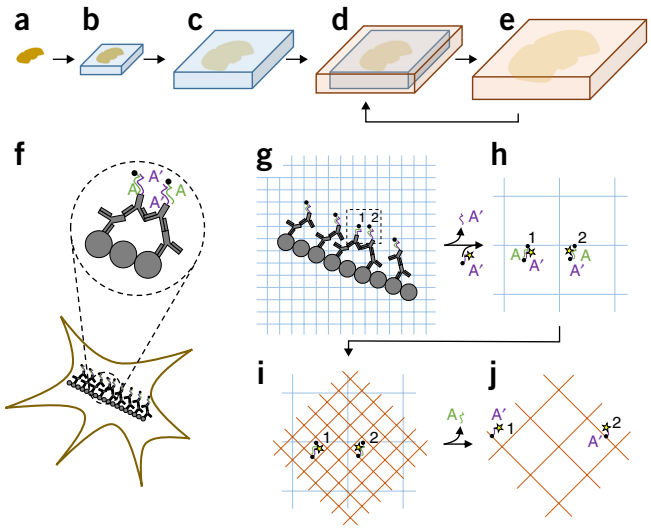

Figure 1 | Iterative expansion microscopy (iExM) concept. (**a**–**e**) Schematic of iterative expansion. (**b**) First, a swellable polyelectrolyte gel network containing a cleavable crosslinker is formed throughout a specimen, then (**c**) it is mechanically homogenized and expanded. (**d**) After expansion, a second swellable polyelectrolyte gel network is formed throughout the first, and then (**e**) it is expanded after dissolving the first gel. (**f**–**j**) Molecular view of the iExM process. (**f**) Biomolecules of interest (gray circles) are first labeled with a primary antibody (shown also in gray) followed by a secondary antibody conjugated to a DNA (purple, sequence A′) molecule, then a complementary DNA (green, sequence A) bearing a gel-anchoring moiety (acrydite, black dot), as in our original ExM procedure[1]. (**g**) The sample (two example biomolecules are labeled "1" and "2," to be followed throughout subsequent diagram panels) is embedded in a cleavable swellable polyelectrolyte gel (blue mesh). This gel incorporates the DNA of sequence A at the gel-anchoring site, and it is expanded. (**h**) A DNA oligo with the original A′ sequence (purple strand) bearing a fluorophore (yellow star) and a new gel-anchoring moiety (acrydite, black dot) is hybridized to the anchored A-sequence DNA (green). (**i**) A second swellable gel (orange mesh) is formed that incorporates the final fluorophore-bearing DNA oligo (sequence A′, purple). (**j**) The gel expands the labels away from each other after digesting the first and re-embedding gel through crosslinker cleavage.

expansion ratios slightly smaller than those of iExM (**Supplementary Note 1**), so in the main text we focus on iExM.

Validation of iterative expansion microscopy resolution and distortion

To validate iExM, we imaged the configuration of biomolecules of known organization, analyzing both the resolution obtained as well as distortion over various length scales. We analyzed microtubules, hollow tubes with an outer diameter of ~25 nm as determined by transmission electron microscopy (TEM)[6], on account of their small size and stereotyped appearance in BS-C-1 cells (**Fig. 2a**, upper left). When imaged with stochastic optical reconstruction microscopy (STORM), hollow microtubule structures were clearly resolved (**Fig. 2a**, lower right; **Fig. 2b**). When the cross-section was fit with a sum of Gaussians, the peak-to-peak distance between the sidewalls was 37.3 ± 4.7 nm (mean ± s.d. throughout; **Fig. 2c**), similar to that of previous super-resolution microscopy studies[7,8]. When these cells were expanded via iExM (**Fig. 2d,e**; ~20× physical magnification), such hollow structures could be resolved with confocal microscopy (or widefield microscopy; **Supplementary Fig. 1a**), which was not possible with earlier ~4.5× expansion factor forms of ExM[1]. For iExM-expanded samples, the average distance between the sidewall peaks was 58.7 ± 10.3 nm (**Fig. 2f**; see **Supplementary Fig. 1b**–**d** for cells processed by hp-iExM). In 3D confocal z-stacks of such cells (see **Fig. 2g** for a single *xy*-plane image and **Fig. 2h** for a single *yz*-plane image reconstructed from the z-stack image shown in **Fig. 2g**), tubular cross-sections of microtubules could easily be seen and characterized (**Fig. 2i**).

To understand the peak-to-peak distances measured by iExM versus those measured by STORM, we took into account the size of the probes used to stain the microtubules in each case. We simulated iExM images of microtubules labeled with DNA-conjugated secondary antibodies (description of simulation in **Supplementary Fig. 2** and **Supplementary Note 2**; simulator code contained in **Supplementary Software**). Using this software, we calculated the inner and outer radii of a cylinder that would contain the ends of DNA oligonucleotides borne by secondary antibodies (**Supplementary Fig. 2**; see **Supplementary Fig. 3** for a sketch of how a typical microtubule equipped with antibodies and DNA might appear). We calculated that the DNA-equipped antibodies of iExM may shift the appearance of target proteins up to ~4.6 nm relative to the position that would be obtained via classical super-resolution microscopy using antibodies lacking DNA (modeled in **Supplementary Fig. 4**; see also **Supplementary Note 3**). Such positional errors could be reduced in the future by using different DNA–antibody conjugation strategies (schematized in **Supplementary Fig. 5**; see also **Supplementary Note 4**).

Using these models, we quantitatively estimated the resolution of the overall iExM process. First, we measured the full width at half maximum (FWHM) of single microtubule sidewalls, deriving a value of 25.8 ± 7.7 nm for the point-spread function (PSF) of the overall iExM process, from staining to gelation and expansion to optical imaging (**Supplementary Fig. 6a**). To attempt to estimate the resolution of the iExM process independent of the label (e.g., focusing on the optical, gelation and expansion components), we deconvolved actual images of microtubule sidewalls by a simulated structure of an idealized DNA–antibody-labeled microtubule sidewall (generated according to the model of **Supplementary Fig. 3**), resulting in the slightly smaller value of 22.3 ± 5.3 nm (**Supplementary Fig. 6b**). Finally, we attempted to isolate just the amount of PSF broadening caused by the gelation and expansion steps specifically. We simulated (**Supplementary Fig. 6a**) how microtubules would be expected to look after staining and optical imaging, assuming that gelation and expansion induced zero error. The resultant PSF was ~6 nm smaller than the actual PSF obtained for the entire iExM process, which suggested that the processes of forming and expanding the multiple gels involved in iExM introduced ~6 nm of additional resolution error, beyond the effects of the antibodies, DNA, and optics (see **Supplementary Note 5**). Such a PSF broadening does not greatly alter the mean peak-to-peak distance between target proteins arranged in a complex (**Supplementary Fig. 6c**), but instead it widens the appearance of small proteins or protein complexes via broadening the PSF of iExM.

In ExM, physical expansion occurs in axial as well as in lateral directions, and thus ExM magnifies specimens along the optical axis as well as in the focal plane[1]. When a *yz*-plane (**Fig. 2h**) was reconstructed from the z-stack image shown in **Figure 2g**, the circular cross-section of a microtubule was resolvable

© 2017 Nature America, Inc., part of Springer Nature. All rights reserved.

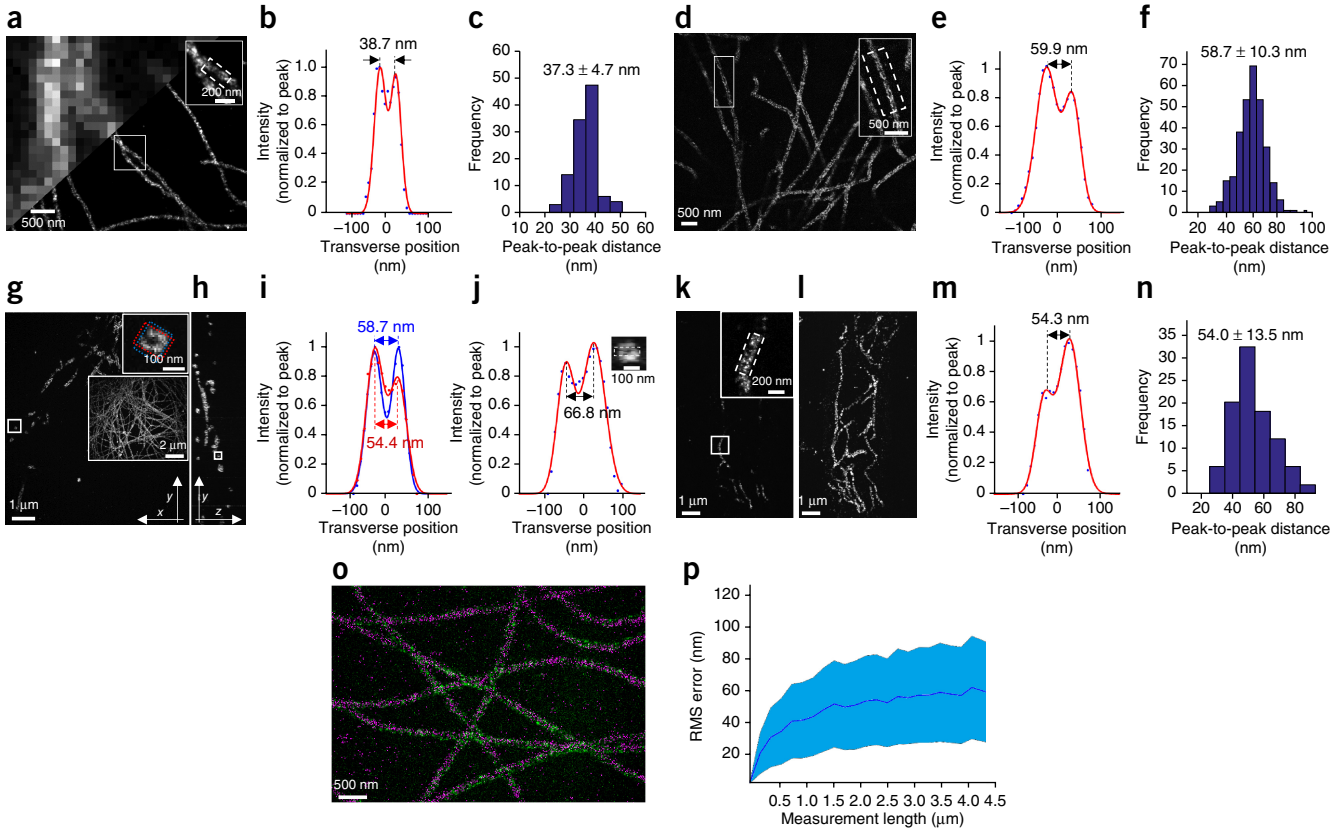

Figure 2 | Validation of the nanoscale precision of iterative expansion microscopy. (**a**–**c**) STORM imaging of cultured BS-C-1 cells after microtubules were labeled with an antitubulin antibody. (**a**) Epifluorescence image (upper left) and STORM image (lower right) of microtubules before expansion. The inset in upper right zooms in on the small box at center. (**b**) Transverse profile of microtubules in the boxed region (dotted lines) of the inset in **a** after averaging down the long axis of the box and then normalizing to the peak value (blue dots), with superimposed fit with a sum of two Gaussians (red lines). (**c**) Population data for 110 microtubule segments from two samples (mean ± s.d.), showing a histogram of peak-to-peak distances. (**d**–**j**) Confocal imaging of cultured BS-C-1 cells with labeled microtubules after ~20-fold expansion via iExM. (**d**) Single *xy*-plane image at the bottom of the cell. The inset in upper right zooms in on the small box at left. (**e**) As in **b**, but for the inset of **d**. (**f**) As in **c**, but for iExM-processed BS-C-1 cells. *n* = 307 microtubule segments from one expanded sample. (**g**) Single *xy*-plane image 1.6 µm above the bottom of the cell. The inset in upper right zooms in on the small box indicated at left, highlighting the circular cross-section of the microtubule (blue and red boxes are used to calculate the profile of **i**). The large inset at right shows the entire cellular context as a maximum intensity projection of the sample. (**h**) Single *yz*-plane within the volume imaged in **g**; the small box is highlighted in the inset of **j**. (**i**) Transverse profiles (i.e., plotting along the long axis of the highlighting box) of the microtubule in the upper right inset of **g**, with color corresponding to that of the highlighting box in the inset. (**j**) Transverse profile of the microtubule in the small box of **h**. Inset, zoomed-in image of the box of **h**, showing the cross-section of the microtubule being resolved along the optical axis. (**k**) Confocal image of a 100-µm-thick slice of mouse cortex with microtubules labeled after ~18-fold expansion via iExM, imaged at a single *xy*-plane. (**l**) Maximum intensity projection of the sample shown in **k**. (**m**) As in **e**, but for the inset of **k**. (**n**) Population data for 96 microtubule segments from one expanded sample, showing a histogram of the peak-to-peak distances. (**o**) Overlay, using only a rigid registration, of a STORM image (magenta) of cultured BS-C-1 cells stained with antitubulin pre-expansion with a confocal image (green) of the same sample postexpansion. (**p**) RMS length measurement error of biological measurements calculated using the distortion vector field method[9] using STORM microscopy pre-expansion followed by confocal imaging of iExM-processed samples (~20× expanded) (blue line, mean; shaded area, ±1 s.d.; *n* = 3 samples).

(**Fig. 2j**, inset). The nanoscale axial resolution of iExM enabled clear visualization of microtubules of BS-C-1 cells in 3D (**Supplementary Videos 1** and **2**).

We applied iExM to preserved mouse tissues—including brain, liver and lung—to determine whether iExM could resolve ~20-nm biological structures in intact tissues. As shown in the inset of **Figure 2k** (single z-plane image; see **Fig. 2l** for the entire cellular context), the sidewalls of microtubules in mouse brain slices were resolvable on a confocal microscope. The distance between the two peaks of the fitted Gaussians was similar to that obtained in the cultured cell case (**Fig. 2m**; population data in **Fig. 2n**). The sidewalls of microtubules in cells of mouse lung and liver tissue slices were also easily resolved on confocal microscopes (**Supplementary Fig. 7a**–**h**). In addition to the visualization of the sidewalls of microtubules in tissues, we found that individual components of microtubule bundles in the mouse cortex could be resolved after 18-fold expansion (**Supplementary Fig. 7i**–**l**).

In addition to resolution, the ability to tell finely spaced objects apart, another optical parameter of interest is distortion across more extended length scales. Accordingly, we quantified the distortion caused by iExM over various length scales that corresponded to feature sizes of interest in cell biology. To measure distortion over scales of several microns, we compared pre-expansion images taken on a super-resolution microscope to postexpansion images taken on a conventional diffraction-limited microscope[1,2,9]. We prepared samples with secondary antibodies labeled

© 2017 Nature America, Inc., part of Springer Nature. All rights reserved.

with STORM dyes and simultaneously applied DNA-conjugated secondary antibodies so they could be processed for iExM and visualized postexpansion. We coregistered the pre-expansion STORM image and postexpansion confocal image via a rigid transformation (**Fig. 2o**), and then we calculated the deformation vector field between the two images[1,2,9]. Although the image qualities enabled by STORM and iExM were compromised in this specific experiment because of the special requirements involved in imaging the same sample for both methods (e.g., each label will occur at half the antibody labeling density of a typical experiment, since we are dual labeling), the root mean square (RMS) alignment error between iExM and STORM was nonetheless small, about 2.5% of measurement length (**Fig. 2p**) over scales of several microns, similar to the 1–4% range of alignment errors previously determined for ExM[1,2,9]. We estimated the distortion of iExM across length scales of tens to hundreds of nanometers by examining the variation of microtubule diameter along 400-nm distances down the long axis of the microtubule. The estimated distortion was found to be 9 nm for cells and 13 nm for tissues (see **Supplementary Note 6** for details).

Nanoscale imaging of synapses

We next explored the utility of iExM in the context of resolving proteins within synapses. To improve brightness of expanded specimens, we pursued signal amplification using either DNA or locked nucleic acid (LNA) probes to increase the number of fluorophores associated with a single gel-anchored oligo (see **Supplementary Fig. 8** for schematic; see also **Supplementary Note 7**). We first examined synapses of cultured mouse hippocampal neurons. We labeled synapses with sets of antibodies that indicate putative excitatory (**Fig. 3a–c**) or inhibitory (**Fig. 3d–f**) synapses—anti-Homer1, anti-Bassoon, and anti-Glutamate receptor 1 (GluR1) for the former; anti-Gephyrin, anti-Bassoon, and anti-Gamma-aminobutyric acid receptor Aα1/anti-Gamma-aminobutyric acid receptor Aα2 ($GABA_AR\alpha1/\alpha2$; labeled with the same oligonucleotide strand) for the latter. It was possible not only to resolve the presynaptic scaffolding protein Bassoon from the postsynaptic scaffolding proteins Homer1 and Gephyrin, but also to resolve proteins within a synaptic compartment—resolving the neurotransmitter receptors GluR1 and $GABA_AR\alpha1/\alpha2$ from their respective postsynaptic scaffolding proteins as well (**Fig. 3c**,**f**). We observed the geometric organization of proteins within synapses to see, for example, how GluR1 proteins sometimes formed ring structures around Homer1 proteins (**Fig. 3g**, dotted circle in the upper right inset) as has been previously reported using STORM[10]. The isotropic 3D nature of iExM expansion allowed us to resolve structures organized along the optical axis of the microscope; for example, we resolved ring structures of GluR1 when the synaptic cleft was parallel to the microscope's optical axis (**Fig. 3g**, dotted circle in the bottom).

We demonstrated the ability of iExM to resolve synaptic structures in the mouse brain. We immunostained a mouse brain slice with antibodies against Bassoon and Homer1, expanded the brain slice 16-fold with iExM, and then imaged putative synapses within four different brain regions (overview in **Fig. 3h**; iExM images taken on a confocal microscope in **Fig. 3i–o**; see **Supplementary Fig. 9** for additional images taken with epifluorescence microscopy). The average distances between Bassoon and Homer1 observed in two regions within primary somatosensory cortex (indicated with Roman numerals i and ii in **Fig. 3h** and highlighted in **Fig. 3i**,**j**) were similar to each other (**Fig. 3p**,**q**) and to Bassoon–Homer distances observed in the dorsal striatum (indicated with Roman numeral iii in **Fig. 3h** and highlighted in **Fig. 3k**; see **Fig. 3r** for the population data). However, a fourth region, the medial pallidum (indicated with Roman numeral iv in **Fig. 3h** and highlighted in **Fig. 3l–o**), exhibited distances between Bassoon and Homer1 that were 50% longer (**Fig. 3s**), suggestive of a different synaptic architecture; furthermore, although putative synapses were evenly distributed in cortex and striatum, synapses in the pallidum were arranged in regularly spaced patterns as if they were tiling a cylindrical target (**Fig. 3l–o**; **Supplementary Video 3**). We used iExM to explore other regional heterogeneities in localization of presynaptic and postsynaptic proteins (**Supplementary Fig. 10** and **Supplementary Video 4**). Thus, iExM may be useful for analyzing the varying nanoscale configurations of proteins across brain circuits and regions, because it can support large-volume imaging with nanoscale precision.

We applied Brainbow adeno-associated viruses (AAVs)[11], in which Cre-expressing neurons are virally transduced to express, in random combinations, subsets of four fluorescent proteins (TagBFP, mTFP, mCherry, and EYFP), each fused to a farnesylation tag for membrane targeting. When such mouse brain slices were immunostained with antibodies against Homer1, as well as against fluorescent proteins (mCherry for **Fig. 3t**; EYFP for **Fig. 3u**), we found that postsynaptic proteins and membrane outlines could be covisualized (**Fig. 3t**,**u**). At synaptic contacts (as indicated by Homer1 staining) we observed less membrane-bound fluorophore (e.g., arrows of **Fig. 3t**,**u**), perhaps because the density of proteins at the synaptic cleft prevents the inward diffusion of membrane-anchored fluorophores. Thus iExM may be useful for mapping out how proteins are arranged in small, even nanoscale, compartments of neurons.

Nanoscale imaging of 3D mouse brain circuitry

We prepared Brainbow-AAV-labeled mouse brain samples as above and performed iExM with locked nucleic acid hybridization-based signal amplification. Brainbow-AAV-labeled dendritic spines in the molecular layer of the mouse hippocampal dentate gyrus are hard to resolve without expansion (**Fig. 4a**). In such samples processed with ~4.5×-expansion-factor protein-retention expansion microscopy (proExM, in which antibodies, genetically encoded fluorophores, or other proteins within a specimen are anchored to the swellable gel and then expanded[2]), dendritic spines could be identified and sometimes even distinguished from one another, but their shapes were difficult to analyze (**Fig. 4b**). After iExM the number, size, position, and shapes of dendritic spines were easily visualized, as is shown in the maximum intensity projection in **Figure 4c** (see **Supplementary Video 5** for 3D visualization; note that as in **Fig. 3t**,**u**, membrane-anchored fluorophores are less dense or even absent at the tips of spines, consistent with membrane-anchored fluorophore exclusion by postsynaptic proteins as hypothesized above; see **Supplementary Fig. 11**). In particular, the hollow space within neurons (**Fig. 4d–f**) and spines was easily visualized when we used membrane-localized fluorescent proteins (**Fig. 4f**; for more examples, see **Supplementary Fig. 12** and **Supplementary Video 6**). With iExM, it is possible to visualize structures such as spines along neural processes that extend over large 3D volumes; for example, along branching dendrites (shown in **Fig. 4g**; four sections of **Fig. 4g**

© 2017 Nature America, Inc., part of Springer Nature. All rights reserved.

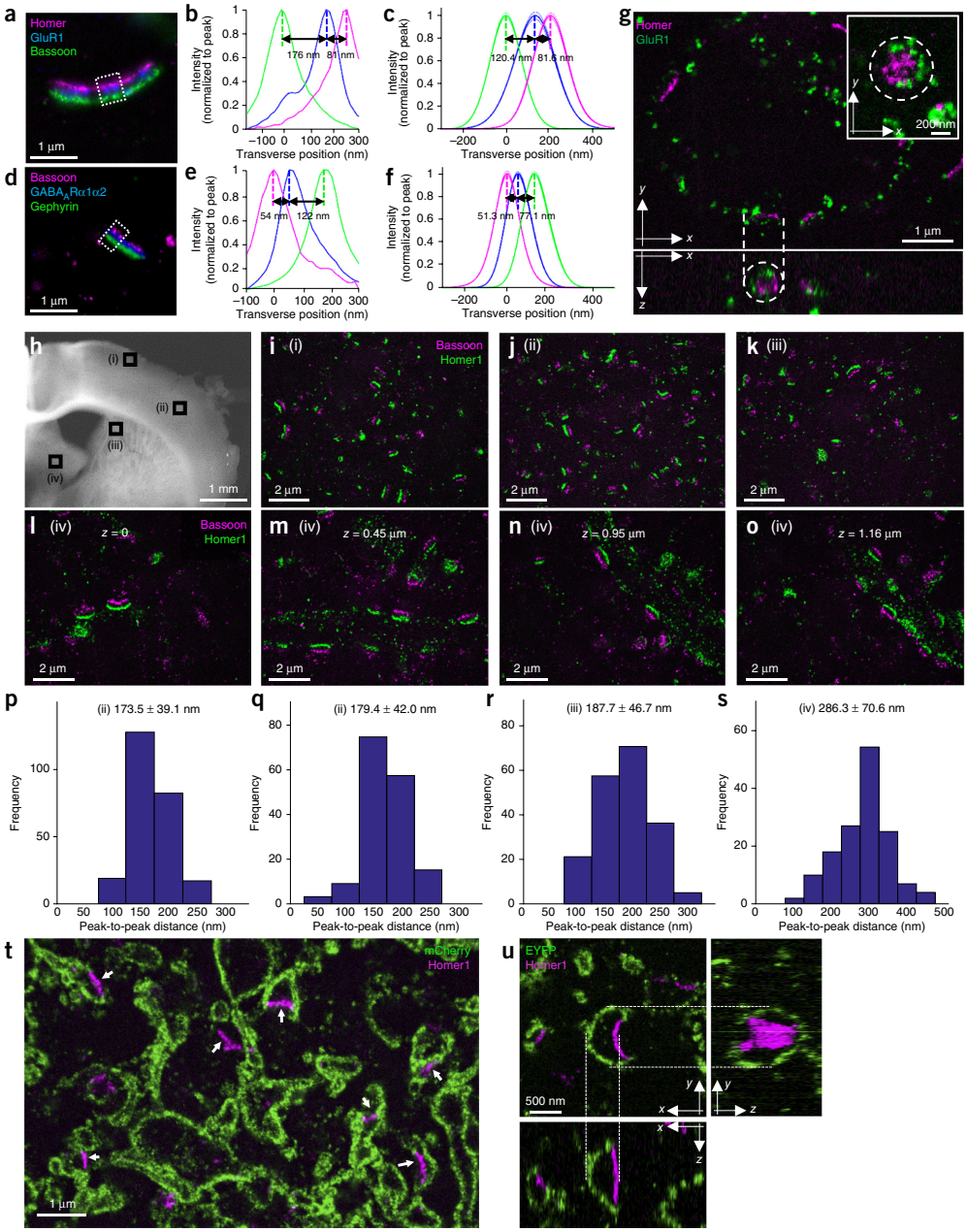

Figure 3 | Nanoscale-resolution imaging of synapses using iExM. (**a**) Epifluorescence image of cultured hippocampal neurons stained with antibodies against Homer1 (magenta), glutamate receptor 1 (GluR1, blue), and Bassoon (green), after ~13-fold expansion via iExM and DNA-hybridization-based signal amplification. Boxed regions are analyzed further in **b**. (**b**) Transverse profile of the three proteins imaged in the sample of **a** (in the boxed region) after normalizing to the peak (Homer1 in magenta, GluR1 in blue, Bassoon in green). (**c**) Sum of Gaussian functions fitted to curves as in **b** for ten synapses from one sample, normalized to peak (thick lines, mean; thin lines, ±1 s.d.). (**d**) As in **a**, but stained with antibodies against Bassoon (magenta), $GABA_AR\alpha1/\alpha2$ (blue), and Gephyrin (green). (**e**) As in **b**, but for the boxed region in **d** (Bassoon in magenta, $GABA_AR\alpha1/\alpha2$ in blue, Gephyrin in green). (**f**) As in **c**, but for the labels of **d**; 14 synapses from one sample. (**g**) Confocal z-stack (top, a single *xy*-plane; bottom, a single *xz*-plane; dotted lines connect corresponding points in the two cross-sections) of cultured hippocampal neurons with labeled Homer1 (magenta) and GluR1(green) after ~20-fold expansion via iExM. Inset of upper panel shows a zoomed-in image of a synapse (from another field of view) showing the circular distribution of GluR1 around Homer1. (**h**) Low-magnification widefield image of a mouse brain slice (corresponding to slide 57 of the Allen Brain Reference Atlas, P56 mouse, coronal sections) showing four regions, i–iv, that were imaged after expansion in **i**–**o** (i and ii, primary somatosensory cortex; iii, dorsal striatum; iv, medial pallidum). (**i**–**k**) Confocal images of three regions, i–iii, highlighted in **h** after labeling with anti-Bassoon (magenta) and anti-Homer1 (green) and 16-fold expansion via iExM. (**l**–**o**) Single *xy*-plane imaged at iv in **h** at different z-heights. (**p**–**s**) Population data of the Homer1–Bassoon separation (mean ± s.d.) measured in the four regions shown in **h**. The number of Homer1–Bassoon pairs analyzed was: **p**, 248 pairs from one specimen; **q**, 159 pairs from one specimen; **r**, 189 pairs from one specimen; **s**, 147 pairs from one specimen. (**t**,**u**) Confocal images of motor cortex areas (**t**, slide 57 of the Allen Brain Reference Atlas P56 mouse coronal sections; **u**, slide 47 of the same Atlas) after immunostaining and expansion. (**t**) Confocal image of the specimen after immunostaining with antibodies against Homer1 (magenta) and mCherry (green) and 16-fold expansion via iExM. (**u**) Z-stack confocal image of the specimen after immunostaining with antibodies against Homer1 (magenta) and EYFP (green) and 20-fold expansion via iExM. Upper left shows a single *xy*-plane image; right shows a single *yz*-plane image reconstructed from the z-stack image; bottom shows a single *xz*-plane image reconstructed from the z-stack image.

© 2017 Nature America, Inc., part of Springer Nature. All rights reserved.

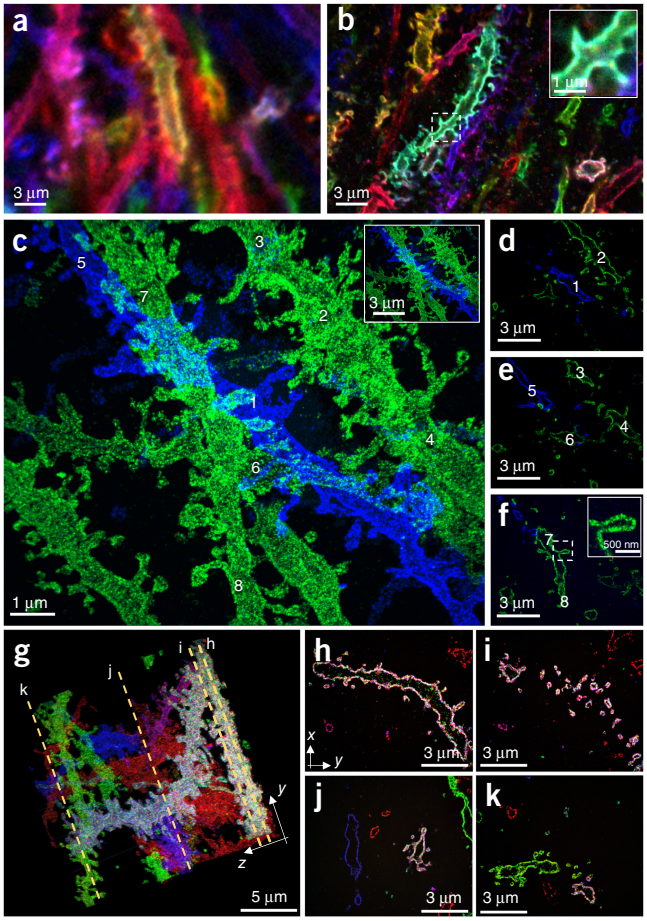

Figure 4 | Nanoscale-resolution imaging of mouse hippocampal brain circuitry. (**a**) Confocal image of immunostained Emx1-Cre mouse hippocampus with neurons expressing membrane-bound fluorescent proteins (Brainbow AAVs) before expansion. Blue, EYFP; red, TagBFP; green, mTFP. (**b**) As in **a**, but expanded 4.5-fold by the antibody-anchoring form of the ProExM protocol[2]. Blue, EYFP; red, TagBFP; green, mTFP. Inset shows a magnified image of a spine in the dotted box of **b**. (**c**–**f**) Confocal z-stack image of 20-fold-expanded mouse hippocampal circuitry with labeled EYFP (blue) and mCherry (green). (**c**) Maximum intensity projection of the stack shown in (**d**–**f**); numbers refer to neural processes that are highlighted within individual z-stacks in **d**–**f**. Inset shows a demagnified view of the image of **c** with the same scale bar as **a** and **b**. (**d**–**f**) Single *xy*-plane images at different z-heights from the bottom of the specimen. (**d**) z = 1.9 µm; (**e**) z = 2.4 µm; (**f**) z = 3.2 µm. See **Supplementary Video 5** for 3D video and surface rendering. Inset of **f** shows a magnified view of a spine in the dotted box of **f**. (**g**–**k**) Confocal z-stack image of 20-fold-expanded mouse hippocampal circuitry with labeled EYFP and mTFP (blue; both EYFP and mTFP were labeled in the same color), mCherry (green), and tagBFP (red). (**g**) Maximum intensity projection of the stack; dotted orange lines highlight four z-planes which yielded the images of **h**–**k**. (**h**–**k**) Single z-plane images of the stack of **g**. See **Supplementary Video 7** for 3D video.

are shown in **Fig. 4h**–**k**; see also **Supplementary Video 7**; further examples in **Supplementary Fig. 13** and **Supplementary Videos 8** and **9**). To some extent, neuronal geometries could even be resolved with epifluorescence microscopy (mouse cortex, 16-fold expansion via hp-iExM; **Supplementary Fig. 14**). Thus, iExM can be used to explore neural connectivity in 3D with spatial precision sufficient for resolving individual synaptic connections.

Can iExM be applied beyond two rounds? In principle we could perform the second round of expansion so that a third round would be possible by using a crosslinker whose cleaving chemistry is orthogonal to that of the first crosslinker. We found that it was possible to magnify a sample by 4.6 × 3.2 × 3.6 ~53-fold (see **Supplementary Note 8** for details; see **Supplementary Fig. 15** for 53-fold-expanded BS-C-1 cells after antibody-labeling tubulin). Although this might seem to imply an effective resolution of 300 nm / 53 = 5.7 nm, the actual resolution is limited by the size of antibodies, the use of DNA anchors (additional ~4.6-nm positional errors, as estimated above), and the broadening of the PSF by the gelation and expansion process (additional ~6 nm errors, as estimated above). However, with nanobody-based[12] or small-molecule tags[13] compatible with iExM, iterated expansion strategies may be able to further improve in resolution beyond 25 nm.

DISCUSSION

iExM achieves resolutions comparable to those of the highest performing forms of super-resolution light microscopy. Although expanded samples prepared with iExM can be quite large, they are transparent and homogeneous in refractive index (since they are 99.99% polymer and water and less than 0.01% original biomaterial), analogous to previous ExM versions[1–3,9], and thus may be amenable to fast, large-volume imaging modalities compatible with transparent tissues such as light-sheet microscopy[14]. Indeed, light-sheet imaging of ExM-processed tissues has recently been shown to be feasible[3]. With objective lenses of working distance ~8 mm available (for example, the Olympus 25× 0.9 NA[15]), ~400-µm-thick slices could be expanded by ~20× and imaged without further sectioning. iExM-processed samples are stiff enough to support postexpansion sectioning (e.g., with a vibratome); any sectioning error is effectively divided by the expansion factor in terms of impact on the biological information, and thus iExM could in principle help support the mapping of neural circuitry over large volumes, for example, entire neural circuits or even entire brains. The volumetric dilution of iExM results in a lower density of biomolecules and labels, but the additional room created by expansion can support amplification chemistries such as those used here or other variants of hybridization-based fluorescence amplification such as the hybridization chain reaction (HCR)[16]. In fact, we recently used HCR in the context of expanded brain tissues to visualize single RNAs within synaptic compartments of neurons in intact mouse brain circuits, taking advantage of the room made by expansion to append on the order of perhaps several dozen fluorophores to a single RNA strand[3].

iExM is a strategy, not a single chemistry, and thus could be applied to other fundamental ExM chemistries—for example, cleavable monomers that could support iterative removal of previous gels, as well as alternative polymer systems[17]. Since iExM concludes with nucleic acid strands (whose sequences code for protein identity) anchored throughout a polymer network at locations determined by the original protein locations, iExM may be able to support multiplexed *in situ* proteomics through serial hybridization of fluorescent strands as is done in DNA-PAINT[18]. We recently demonstrated serial hybridization readout of multiple RNAs using our ExFISH variant of ExM[3]. Because iExM decrowds protein labels to the point where signals become discontinuous as individual labels are separated, coded hybridization strategies where the same strand is imaged many times with different sets of probes may allow an exponential

© 2017 Nature America, Inc., part of Springer Nature. All rights reserved.

number of proteins to be probed given a linear number of hybridization rounds—as has been previously done with RNA[19,20]. The additional room around biomolecules created by expansion could enable potentially complex reactions, including sequencing[21], to be conducted on expanded tissues, furthering the ability to read out the molecular composition of complex biological systems in a multiplexed, yet scalable, way. Finally, direct-anchoring versions of iExM may be possible, in which proteins or other biomolecules are directly anchored to the swellable polymer and then moved away from each other through repeated physical expansion. To achieve this, it would be important to develop ways to transfer the anchored biomolecules from the first swellable gel to the second. For example, in protein retention expansion microscopy (proExM), proteins (potentially including antibodies or fluorescent proteins) are directly anchored to the polymer gel and then expanded away from each other[2,9,22]; to create an iterative form of proExM, one would need novel chemical linkers that can support the covalent transfer of the proteins from the first gel to the second.

METHODS

Methods, including statements of data availability and any associated accession codes and references, are available in the online version of the paper.

Note: Any Supplementary Information and Source Data files are available in the online version of the paper.

ACKNOWLEDGMENTS

E.S.B. was funded by the HHMI-Simons Faculty Scholars Program; the NIH Director's Pioneer Award 1DP1NS087724; the New York Stem Cell Foundation-Robertson Award; the US Army Research Laboratory and the US Army Research Office under contract/grant number W911NF1510548; US-Israel Binational Science Foundation Grant 2014509; the Picower Institute Innovation Fund; IARPA D16PC00008; NIH grants 1R01MH110932, 1R43MH101943, 1R01MH103910, 1R01EY023173, and 2R01DA029639; the IET A.F. Harvey Prize; the Open Philanthropy Project; the Halis Family Foundation; and the MIT Media Lab. J.-B.C. was supported by the Simons Postdoctoral Fellowship. F.C. was supported by the NSF Fellowship and Poitras Fellowship. Y.-G.Y., J.S.K., and H.-J.S. were supported by Samsung Scholarships. P.W.T. and A.T.W. were supported by Hertz Foundation fellowships. Confocal imaging was performed in the W.M. Keck Facility for Biological Imaging at the Whitehead Institute for Biomedical Research J.-B.C. was supported by the Center for Neuroscience Imaging Research. D.C. was funded by NIH grants R21GM114852 and R01MH110932. We acknowledge W. Salmon (MIT) for her assistance with confocal imaging. STORM imaging shown in **Figure 2o** was performed in the Center for Brain Science at Harvard University. We acknowledge E. Garner, C. Wivagg, and S. Turney (Harvard) for allowing us to use the N-STORM microscope and their assistance with STORM imaging. We acknowledge D. Park (MIT) for assistance with the preparation of cultured neurons. We also acknowledge S. Shim, Y. Sigal, C. Speer, M. Thanawala, D. Kim, M. Sauer, and S. Alon for helpful discussions. We acknowledge University of Michigan, Ann Arbor for providing antibodies against Brainbow fluorescent proteins.

AUTHOR CONTRIBUTIONS

E.S.B. and J.-B.C. conceived the main idea and designed experiments. P.W.T. conceived hp-iExM strategy. J.-B.C. performed immunostaining and expanded specimens. J.-B.C., F.C., and A.W. developed re-embedding process. J.-B.C. calculated RMS error of iExM. F.C. conceived signal amplification methods. E.E.J. performed immunostaining. Y.-G.Y. performed deconvolution and denoising and developed the iExM simulator. H.-J.S. and N.P. performed the brainbow virus injection and perfusion. Y.-G.Y. and S.A. created 3D videos. H.B. contributed STORM data in **Figure 2a–c**. J.-B.C. performed STORM imaging for **Figure 2o,p**. D.C. provided antibodies against Brainbow fluorescent proteins. J.-B.C. and J.S.K. imaged samples and performed image processing. J.-B.C. performed statistical analysis. E.S.B. and J.-B.C. wrote the paper. All authors contributed to editing of the paper. E.S.B. supervised this work.

COMPETING FINANCIAL INTERESTS

The authors declare competing financial interests: details are available in the online version of the paper.

Reprints and permissions information is available online at http://www.nature.com/reprints/index.html. Publisher's note: Springer Nature remains neutral with regard to jurisdictional claims in published maps and institutional affiliations.

1. Chen, F., Tillberg, P.W. & Boyden, E.S. Expansion microscopy. *Science* **347**, 543–548 (2015).
2. Tillberg, P.W. *et al.* Protein-retention expansion microscopy of cells and tissues labeled using standard fluorescent proteins and antibodies. *Nat. Biotechnol.* **34**, 987–992 (2016).
3. Chen, F. *et al.* Nanoscale imaging of RNA with expansion microscopy. *Nat. Methods* **13**, 679–684 (2016).
4. O'Connell, P.B.H. & Brady, C.J. Polyacrylamide gels with modified cross-linkages. *Anal. Biochem.* **76**, 63–73 (1976).
5. Kurenkov, V.F., Hartan, H.-G. & Lobanov, F.I. Alkaline hydrolysis of polyacrylamide. *Russ. J. Appl. Chem.* **74**, 543–554 (2001).
6. Weber, K., Rathke, P.C. & Osborn, M. Cytoplasmic microtubular images in glutaraldehyde-fixed tissue culture cells by electron microscopy and by immunofluorescence microscopy. *Proc. Natl. Acad. Sci. USA* **75**, 1820–1824 (1978).
7. Dempsey, G.T., Vaughan, J.C., Chen, K.H., Bates, M. & Zhuang, X. Evaluation of fluorophores for optimal performance in localization-based super-resolution imaging. *Nat. Methods* **8**, 1027–1036 (2011).
8. Aquino, D. *et al.* Two-color nanoscopy of three-dimensional volumes by 4Pi detection of stochastically switched fluorophores. *Nat. Methods* **8**, 353–359 (2011).
9. Chozinski, T.J. *et al.* Expansion microscopy with conventional antibodies and fluorescent proteins. *Nat. Methods* **13**, 485–488 (2016).
10. Dani, A., Huang, B., Bergan, J., Dulac, C. & Zhuang, X. Superresolution imaging of chemical synapses in the brain. *Neuron* **68**, 843–856 (2010).
11. Cai, D., Cohen, K.B., Luo, T., Lichtman, J.W. & Sanes, J.R. Improved tools for the Brainbow toolbox. *Nat. Methods* **10**, 540–547 (2013).
12. Olivier, N., Keller, D., Gönczy, P. & Manley, S. Resolution doubling in 3D-STORM imaging through improved buffers. *PLoS One* **8**, e69004 (2013).
13. Wombacher, R. & Cornish, V.W. Chemical tags: applications in live cell fluorescence imaging. *J. Biophotonics* **4**, 391–402 (2011).
14. Chen, B.-C. *et al.* Lattice light-sheet microscopy: imaging molecules to embryos at high spatiotemporal resolution. *Science* **346**, 1257998 (2014).
15. Ke, M.-T., Fujimoto, S. & Imai, T. SeeDB: a simple and morphology-preserving optical clearing agent for neuronal circuit reconstruction. *Nat. Neurosci.* **16**, 1154–1161 (2013).
16. Choi, H.M.T. *et al.* Programmable *in situ* amplification for multiplexed imaging of mRNA expression. *Nat. Biotechnol.* **28**, 1208–1212 (2010).
17. Cipriano, B.H. *et al.* Superabsorbent hydrogels that are robust and highly stretchable. *Macromolecules* **47**, 4445–4452 (2014).
18. Jungmann, R. *et al.* Multiplexed 3D cellular super-resolution imaging with DNA-PAINT and Exchange-PAINT. *Nat. Methods* **11**, 313–318 (2014).
19. Lubeck, E., Coskun, A.F., Zhiyentayev, T., Ahmad, M. & Cai, L. Single-cell *in situ* RNA profiling by sequential hybridization. *Nat. Methods* **11**, 360–361 (2014).
20. Chen, K.H., Boettiger, A.N., Moffitt, J.R., Wang, S. & Zhuang, X. RNA imaging. Spatially resolved, highly multiplexed RNA profiling in single cells. *Science* **348**, aaa6090 (2015).
21. Lee, J.H. *et al.* Highly multiplexed subcellular RNA sequencing. *in situ*. *Science* **343**, 1360–1363 (2014).
22. Ku, T. *et al.* Multiplexed and scalable super-resolution imaging of three-dimensional protein localization in size-adjustable tissues. *Nat. Biotechnol.* **34**, 973–981 (2016).

© 2017 Nature America, Inc., part of Springer Nature. All rights reserved.

ONLINE METHODS

A step-by-step protocol of this method can be found in the **Supplementary Protocol**. A table of all chemicals can be found in **Supplementary Table 1**.

DNA, locked nucleic acids, and primary and secondary antibody preparation. Oligonucleotides were purchased from Integrated DNA technologies (IDT) with standard desalting purification (see **Supplementary Tables 2–8** for the sequences). Locked nucleic acids (LNAs) were purchased from Exiqon with high-performance liquid chromatography (HPLC) purification (see **Supplementary Table 9** for the sequences). Primary and secondary antibodies were purchased from multiple vendors (see **Supplementary Tables 10–12**). Primary antibodies used were rabbit anti-beta tubulin (Abcam ab6046, 1:100), rabbit anti-Homer1 (Synaptic systems 160003, 1:200), guinea pig anti-Homer1 (Synaptic systems 160004, 1:200), mouse anti-Homer1 (Synaptic systems 160011, 1:200), mouse anti-Bassoon (Enzo ADI-VAM-PS003-F, 1:200), guinea pig anti-Bassoon (Synaptic systems 141004, 1:200), mouse anti-Gephyrin (Synaptic systems 147011, 1:200), rabbit anti-$GABA_AR\alpha1$ (Synaptic systems 224203, 1:200), rabbit anti-$GABA_AR\alpha2$ (Synaptic systems 224103, 1:200), rabbit anti-GluR1 (Abcam ab31232, 1:100), guinea pig anti-TagRFP (Kerafast EMU107, 1:200), rabbit anti-mCherry (Abcam ab167453, 1:200), rat anti-mCherry (ThermoFisher M11217, 1:200), rat anti-mTFP (Kerafast EMU103, 1:200), and chicken anti-GFP (Kerafast EMU101, 1:400). Secondary antibodies used were goat anti-chicken (ThermoFisher A-11039, 10 μg/μL), goat anti-rat (ThermoFisher A-11081, 10 μg/μL), goat anti-guinea pig (Biotium CF633 conjugated, 10 μg/μL), and donkey anti-rabbit (ThermoFisher A31573, 1:100). Secondary antibodies from Jackson ImmunoResearch were used to make DNA-conjugated secondary antibodies, using the following reagents: donkey anti-rabbit (711-005-152), donkey anti-chicken (703-005-155), donkey anti-rat (712-005-153), donkey anti-guinea pig (706-005-148), and donkey anti-mouse (715-005-151). For DNA-conjugated secondary antibodies, 10 μg/μL was used for cultured cell lines/neurons, and 20 μg/μL was used for tissue slices. Oligonucleotides with a 5′ amine modification (see **Supplementary Table 2** for the sequences) were conjugated to secondary antibodies using a modified protocol from a commercial kit (Solulink, Antibody-Oligonucleotide All-in-One conjugation kit; please visit http://expansionmicroscopy.org/ to find step-by-step instructions for the DNA–antibody conjugation).

Cultured BS-C-1 cell preparation. BS-C-1 cells (American Type Culture Collection, product number CCL-26) were cultured in Nunc Lab-Tek II chambered coverglasses (ThermoFisher, 155409) with Eagle's Minimum Essential Medium supplemented with 10% heat-inactivated fetal bovine serum (FBS) and 1% penicillin–streptomycin, and the cells were incubated at 37 °C in 5% CO_2.

Cultured hippocampal neuron preparation. Hippocampal neurons were prepared from postnatal day 0 or day 1 Swiss Webster (Taconic) mice as previously described[23,24], but with the following modifications. Hippocampal tissues were isolated and digested with 50 units of papain for 6–8 min, and then the digestion was stopped with ovomucoid trypsin inhibitor. 10,000–20,000 cells were plated in Matrigel (BD Biosciences)-coated 96-well glass-bottom plates with 100 μL of plating medium containing MEM (Life Technologies), glucose (33 mM, Sigma), transferrin (0.01%, Sigma), Hepes (10 mM), Glutagro (2 mM, Corning), insulin (0.13%, Millipore), B27 supplement (2%, Gibco), and heat-inactivated FBS (7.5%, Corning). AraC (0.002 mM, Sigma) was added when glial density reached 50–70% of confluence. Neurons were cultured at 37 °C in humidified 5% CO_2.

Brainbow AAV injection and brain preparation. All the following procedures involving animals were approved by the Massachusetts Institute of Technology Committee on Animal Care and were in accordance with the National Institutes of Health Guide for the Care and Use of Laboratory Animals. 4 Emx1-Cre mice ages ~3–5 months old were used. Mice were used without regard for sex. Brainbow rAAV (AAV9.hEF1a.lox.TagBFP.lox.eYFP.lox.WPRE.hGH-InvBYF and AAV9.hEF1a.lox.mCherry.lox.mTFP1.lox.WPRE.hGH-InvCheTF; University of Pennsylvania, Penn Vector Core) was injected into Emx1-Cre mice[11]. Adult Emx1-Cre mice were first head fixed to a stereotaxic apparatus, and a small (~0.5 mm^2) craniotomy was performed under continuous isoflurane anesthesia. A 34-gauge injection needle preloaded with the AAV solution (7.5×10^{12} genome copy/mL) was then inserted into the brain to a depth of ~500 μm from the cortical surface, and the virus was infused at a rate of 0.2 μL/min. After injecting 2 μL of the virus solution, the needle was left at the injection site for an additional 5 min to allow for viral diffusion. Mice were allowed to recover from surgery and express virus for 3–4 weeks before transcardial perfusion. Using isoflurane, mice were deeply anesthetized and perfused with 30 mL room temperature 1× PBS, and then 30 mL room-temperature fixative solution (4% paraformaldehyde in 1× PBS). Brains were then harvested and stored in the same fixative at 4 °C for 24 h. 100-μm- or 150-μm thick brain slices were prepared by slicing brains with 100 mM glycine in 1× PBS on a vibratome (Leica VT1000s). The slices were stored in 1× PBS at 4 °C until staining.

Immunostaining of tissues (except the microtubule staining of mouse tissue slices). All following steps were conducted at room temperature with gentle shaking, unless otherwise noted. To stain Brainbow slices, two different conditions were used. To stain only Brainbow AAV fluorescent proteins (FPs), Brainbow mouse brain slices were first permeabilized and blocked in '0.5T' blocking buffer (0.5% Triton X-100, 5% normal donkey serum (NDS), 1× PBS) for 2 h. Slices were then incubated with primary antibodies (see **Supplementary Tables 10** and **11** for details) in '0.25T' blocking buffer (0.25% Triton X-100, 5% NDS, 1× PBS) for 2–3 d at 4 °C with gentle shaking. Slices were washed in 0.25T blocking buffer four times for 30 min each time. Slices were incubated with DNA-conjugated secondary antibodies in hybridization buffer (2× SSC buffer, 10% dextran sulfate, 1 mg/mL yeast tRNA, 5% NDS, 0.1% Triton X-100) overnight and washed in 0.25T blocking buffer four times for 30 min each time. Slices were then incubated with DNAs with a 5′ acrydite modification at a concentration of 1 ng/μL in hybridization buffer overnight, and then they were washed in 0.25T blocking buffer four times for 30 min each time.

To stain synaptic proteins, or synaptic proteins and Brainbow FPs, Brainbow slices were first permeabilized and blocked in '0.1T' blocking buffer (0.1% Triton X-100, 1× PBS, 5% NDS) for 2 h. Primary antibody staining and subsequent washing steps

© 2017 Nature America, Inc., part of Springer Nature. All rights reserved.

doi:10.1038/nmeth.4261

were identical to those of the FP staining protocol described above, but they were conducted in 0.1T blocking buffer. DNA-conjugated antibody and DNA-staining steps were identical to those of the FP staining protocol. Subsequent washing steps were conducted in 0.1T blocking buffer. To stain FPs for proExM the permeabilization, primary antibody staining, washing steps, and secondary antibody staining were conducted in 0.1T blocking buffer.

Immunostaining of tubulin in cultured cells and tissue slices. All of the following steps were conducted at room temperature, unless otherwise noted. Cells were first washed in 1× PBS three times; then they were extracted in cytoskeleton extraction buffer[25] (0.2% Triton X-100, 0.1 M 1,4-piperazinediethanesulfonic acid (PIPES), 1 mM ethylene glycol-bis(2-aminoethylether)-N,N,N′,N′-tetraacetic acid (EGTA), 1 mM magnesium chloride, pH 7.0) for 1 min and then fixed in tubulin fixation solution (3% formaldehyde, 0.1% glutaraldehyde, 1× PBS) for 10 min, followed by reduction with 0.1% sodium borohydride in 1× PBS for 7 min and washing with 100 mM glycine in 1× PBS three times for 5 min each time. Cells were permeabilized and blocked in 0.2T blocking buffer (0.2% Triton X-100, 1× PBS, 5% NDS) for 10 min and incubated with rabbit anti-beta tubulin antibody in '0.2T' blocking buffer at a concentration of 10 μg/mL for 1 h, and then they were washed in 1× PBS three times. Cells were incubated with DNA-conjugated anti-rabbit secondary antibody (RbA1′ in **Supplementary Table 12**) in hybridization buffer at a concentration of 10 μg/mL for 1 h with gentle shaking, then they were washed in 1× PBS three times. Cells were incubated with DNA (A1 5′ acrydite 3′ Alexa 488 in **Supplementary Table 3**) in hybridization buffer at a concentration of 0.5 ng/μL for 1 h with gentle shaking, then they were washed three times in 1× PBS.

To stain microtubules of mouse tissue slices, Thy1–YFP mice were deeply anesthetized using isoflurane and perfused with 30 mL room temperature 1× PBS. Brains, livers, and lungs were then harvested and sliced on a vibratome (Leica VT1000s) to a thickness of 100 μm in 1× PBS. Slices were extracted in cytoskeleton extraction buffer[25] for 5 min with gentle shaking, and then they were fixed in tubulin fixation solution for 30 min with gentle shaking, followed by reduction with 0.1% sodium borohydride in 1× PBS for 7 min with gentle shaking and washing with 100 mM glycine in 1× PBS three times with gentle shaking for 10 min each time.

Slices were permeabilized and blocked in 0.2T blocking buffer (0.2% Triton X-100, 5% NDS, 1× PBS) for 2 h with gentle shaking. Primary antibody staining and all washing steps were identical to those of the the synaptic protein staining protocol, but they were conducted in 0.2T blocking buffer. DNA-conjugated antibody and DNA staining steps were identical to those of the synaptic protein staining protocol.

Immunostaining of synaptic proteins in cultured neurons. All following steps were conducted at room temperature, unless otherwise noted. Cultured neurons were fixed 2 weeks after initial plating. Cultured neurons were first washed in 1× PBS three times, and then they were fixed with 4% formaldehyde in 1× PBS for 10 min and washed with 100 mM glycine in 1× PBS three times for 5 min each time. Subsequent procedures were identical to the microtubule staining of cultured cells.

First-round expansion except for triple-round expansion experiments. After immunostaining, cultured cells, neurons, and tissue slices were first incubated in pregel incubation solution (see **Supplementary Table 13** for details) overnight at 4 °C. After the incubation, specimens were incubated in 1st gelation solution (**Supplementary Table 13**) twice for 30 min each time at 4 °C. For cultured cells and neurons, 200 μL of 1st gelation solution was added to each well and then incubated at 37 °C for 3 h. For tissue slices, slices were placed between two pieces of no. 1 coverglass separated by another no. 1 coverglass, and then they were incubated at 37 °C for 3 h.

After the incubation, gels (including cultured cells, neurons, and tissue slices) were incubated with Proteinase K at a concentration of 8 units/mL (1:100 dilution) in digestion buffer (50 mM Tris pH 8, 1 mM EDTA, 0.5% Triton-X100, 0.8 M guanidine HCl) overnight at room temperature with gentle shaking. Digested gels were next placed in an excess volume of fresh distilled (DI) water for three periods (2 h, 2 h, overnight) at room temperature with gentle shaking.

Re-embedding and DNA hybridization except for triple-round expansion experiments. All of the following steps were conducted at room temperature with gentle shaking, unless otherwise noted. Expanded gels were incubated in a freshly prepared re-embedding solution (**Supplementary Table 13**) twice for 30 min each time. After the incubation, gels were placed between two pieces of no. 1 coverglass and then incubated at 37 °C for 1.5 h in a nitrogen-filled chamber. Following the incubation, gels were detached from the coverglass and then washed in DNA hybridization buffer (20% (v/v) formamide in 4× saline-sodium citrate (SSC) buffer) for 30 min to remove any unreacted monomers from gels.

Gels that would not undergo signal amplification were incubated with DNAs (see **Supplementary Tables 4** and **10** for details) at a concentration of 0.5 ng/μL in DNA hybridization buffer overnight, and then they were washed in DNA hybridization buffer three times, for 2 h, 2 h, and overnight.

Gels that would undergo DNA- or LNA-hybridization-based signal amplification were incubated with linker DNAs (see **Supplementary Tables 4** and **10** for details) at a concentration of 2 ng/μL in DNA hybridization buffer overnight, and then they were washed in DNA hybridization buffer three times, for 2 h, 2 h, and overnight.

Second-round expansion except for triple-round expansion experiments. All of the following steps were conducted at room temperature with gentle shaking, unless otherwise noted. For hp-iExM, gels were incubated in a freshly prepared hp-iExM 2nd gel solution (**Supplementary Table 13**) twice for 30 min each. After this incubation, gels were placed between two pieces of no. 1 coverglass and then incubated in a nitrogen-filled chamber at 37 °C for 1.5 h. After this incubation, gels were incubated in 0.2 M NaOH overnight and washed in DI water multiple times until the size of the gels plateaued.

For iExM, gels were incubated in a freshly prepared iExM 2nd gel solution (**Supplementary Table 13**) twice for 30 min minutes each. After this incubation, gels were placed between two pieces of no. 1 coverglass, and then they were incubated in a nitrogen-filled chamber at 37 °C for 1.5 h. After this incubation, gels were

© 2017 Nature America, Inc., part of Springer Nature. All rights reserved.

incubated in 0.2 M NaOH for 1 h. Gels were washed in DNA hybridization buffer twice for 30 min each time, and then they were incubated with fluorophore-tagged DNAs for DNA-hybridization-based signal amplification and fluorophore-tagged LNAs for LNA-hybridization-based signal amplification at a concentration of 0.5 ng/μL in DNA hybridization buffer overnight, and then they were washed in DNA hybridization buffer three times (2 h, 2 h, and overnight). Gels were then washed in 0.2× PBS multiple times for DNA-hybridization-based signal amplification and in DI water for LNA-hybridization-based signal amplification until the size of the gels plateaued.

Protein retention expansion microscopy. Immunostained brain slices were first incubated in 6-((acryloyl)amino)hexanoic acid, succinimidyl ester (AcX; resuspended in anhydrous DMSO at a concentration of 10 mg/mL and then diluted in 1× PBS at a concentration of 0.1 mg/mL) at room temperature overnight with gentle shaking. Slices were then incubated in monomer solution (1× PBS, 2 M NaCl, 8.625% (w/w) sodium acrylate, 2.5% (w/w) acrylamide, 0.15% (w/w) N,N′-methylenebisacrylamide (BIS), 0.2% (w/w) ammonium persulfate (APS), 0.2% (v/v) tetramethylethylenediamine (TEMED), 0.01% (w/w) 4-hydroxy-2,2,6,6-tetramethylpiperidin-1-oxyl (H-TEMPO)) twice for 30 min each time at 4 °C and placed between two pieces of no. 1 coverglass separated by another no. 1 coverglass and then incubated in a humidified 37 °C incubator for 2 h. Following the incubation, gels were digested in Proteinase K at a concentration of 8 units/mL in 50 mM Tris (pH 8) with 1 mM EDTA, 0.5% Triton X-100, and 1 M NaCl overnight at room temperature with gentle shaking and then expanded in DI water several times until the size of gels plateaued.

Imaging. Imaging was performed on an Andor spinning disk confocal microscope with a 40× 1.15 NA water-immersion objective (**Fig. 2d**,**g**,**k**,**l**,**o**; **Fig. 3g**,**i–o**,**t**,**u**; **Fig. 4**; **Supplementary Figs. 1b**,**2b**,**7**, and **10–13**) or Nikon Eclipse Ti inverted microscope with the same objective (**Fig. 3a**,**d**,**h**; **Supplementary Figs. 1a**,**9**,**14**, and **15**). Background of images was corrected by using the 'subtract background' function implemented in Fiji with a 50-pixel-wide 'rolling ball' algorithm.

Expansion factor measurement. To determine the expansion factors for each round of expansion, we imaged whole specimens (tissues and cultured cells) with a widefield microscope before versus after the expansion of the first gel. The expansion factor for the first round was then determined by measuring the distance between two landmarks in the specimen before versus after the first round of expansion. The expansion factor of the second round was determined in the same way.

Root mean square error measurement. RMS error measurement was performed in a similar way to that of previous studies[1,9]. Briefly, STORM images before expansion and confocal images after expansion were registered using rigid body registration as implemented in Fiji (Plugins → Registration → TurboReg → Rigid Body/Accurate/Manual)[1]. After the registration, deformation vector fields were calculated by using Elastix and Transformix as in ref. 9 (see Supplementary Protocol 1 of ref. 9 for details).

Deconvolution and denoising. Images shown in **Figure 2g** were deconvolved using custom-written MATLAB code that uses the Richardson–Lucy algorithm with wavelet regularization and a theoretical point-spread function. The deconvolution was performed with a GPU (NVidia, Tesla K40c). For **Figure 4c–k**, **Supplementary Figures 10–13**, and **Supplementary Videos 5–9**, the images were first deconvolved, and then the background and signals from nonspecifically bound fluorophores were removed by using connected component analysis[26].

Stochastic optical reconstruction microscopy imaging. BS-C-1 cells were cultured, extracted, fixed, and stained with a primary antibody as in "Immunostaining of tubulin in cultured cells and tissue slices." For **Figure 2a–c**, primary-antibody-stained cells were incubated with Alexa 647 conjugated anti-rabbit antibody (ThermoFisher A-31573, 20 μg/μL) in 0.2T blocking buffer for 30 min, and they werewashed in 1× PBS three times. STORM imaging was performed in STORM imaging buffer (100 mM Tris, pH 8.0, 50 mM NaCl, 1% β-Mercaptoethanol, 5% glucose, 1 μg/μL glucose oxidase, 40 μg/mL catalase) on a custom-built STORM microscope using the oblique-incidence geometry. For **Figure 2o**, primary-antibody-stained cells were incubated with a mixture of Alexa-647-conjugated anti-rabbit secondary antibody (13.3 μg/mL) and DNA-conjugated anti-rabbit secondary antibody (13.3 μg/mL, RbA1′) in hybridization buffer for 1 h at room temperature with gentle shaking and then washed in 1× PBS three times. After the washes, STORM imaging was performed on a commercial Nikon N-STORM microscope in total internal reflection fluorescence (TIRF) mode in STORM imaging buffer (1 M Tris, pH 8.0, 50 mM NaCl, 1% β-Mercaptoethanol, 5% glucose, 1 μg/μL glucose oxidase, 40 μg/mL catalase). After STORM imaging, cells were washed in 1× PBS and then incubated with DNA (A1 5′ acrydite 3′ Alexa 488 in **Supplementary Table 3**) in hybridization buffer at a concentration of 0.5 ng/μL for 1 h at room temperature with gentle shaking then washed three times in 1× PBS.

Statistics. In this study, the sample sizes were decided not based upon a power analysis, since the goal was to develop a new technology. As noted in ref. 27, "in experiments based on the success or failure of a desired goal, the number of animals required is difficult to estimate." As was also noted in this paper, "the number of animals required is usually estimated by experience instead of by any formal statistical calculation, although the procedures will be terminated [when the goal is achieved]."[27] The sample sizes of this study reflect our past experience in developing ExM technologies[1–3]. For animal studies, sample-size estimation was not performed. Exclusion, randomization, and blinding of samples were not performed.

Triple-round expansion. All following steps were conducted at room temperature with gentle shaking, unless otherwise noted. Immunostaining of BS-C-1 cells, pregel incubation, first-gel synthesis, re-embedding, and second-gel synthesis steps were identical to those of the iExM procedure for BS-C-1 cells with labeled tubulin, but with the following modifications. RbB1′ and DNA B1 5′ acrydite were used during the staining step. Pregel incubation solution, 1st gel solution, and 1st re-embedding solution shown in **Supplementary Table 14** were used to form a 1st

© 2017 Nature America, Inc., part of Springer Nature. All rights reserved.

doi:10.1038/nmeth.4261

swellable gel and re-embedding gel. After the re-embedding, gels were incubated with DNA B1′ A2 5′ acrydite (**Supplementary Table 8**). 2nd gel solution shown in **Supplementary Table 14** was used to form a 2nd swellable gel.

After the 2nd gel formation, gels were incubated in 0.25 M tris (2-carboxyethyl)phosphine (TCEP; 1 M stock solution of TCEP diluted in 1 M Tris–HCl pH 8.0) overnight and then expanded in DI water three times. Expanded gels were re-embedded again in 2nd re-embedding solution (**Supplementary Table 14**), incubated with a linker DNA (A2′ 4LNA-A1′ 5′ acrydite) in DNA hybridization buffer overnight at a concentration of 2 ng/μL, and then washed in DNA hybridization buffer three times for 2 h, 2 h, and overnight.

Gels were then embedded in 3rd gel solution (**Supplementary Table 14**) and digested in 0.2 M NaOH for 1 h. Gels were then washed in DNA hybridization buffer and incubated with fluorophore-tagged LNA (LNA-A1 3′atto 565) at a concentration of 0.5 ng/μL in DNA hybridization buffer overnight, and then they were washed in DNA hybridization buffer three times for 2 h, 2 h, and overnight. Gels were then washed in DI water multiple times.

MATLAB simulation of iterative expansion microscopy images. We developed a simulator of iExM images of microtubules labeled with DNA-conjugated secondary antibodies (code contained in **Supplementary Software** and described in **Supplementary Fig. 2**). Simulation of iExM was performed by first creating a cylinder with an inner radius of R_i and outer radius of R_o. 5′ acrydite moieties were randomly assigned to voxels within the cylindrical volume to simulate the stochastic staining of a microtubule. To gauge the impact of the broadening of the PSF on the simulation (**Supplementary Fig. 6c**), the positions of the 5′ acrydite moieties were randomly perturbed with an s.d. E_p (parameter 'PositionE' in the MATLAB code). Then, the cylindrical volume was projected onto a 3D image stack by convolving the volume with the 3D point-spread-function (PSF) of a confocal microscope with an objective lens of 40× magnification and 1.15 NA. Then the volume was down sampled by pixel binning in the lateral dimension (with a pixel size of 6 nm) and subsampled in the axial dimension to incorporate the pixel pitch and the z-step size of the microscope. The simulation was performed multiple times with varying R_i and R_o.

Once the microtubule profiles with various combinations of R_i and R_o were generated, we fitted the simulated profiles with a sum of two Gaussians, and the peak-to-peak distances of the fitted sum of two Gaussians were measured. The measured peak-to-peak distances were compared with the peak-to-peak distances of each experimental microtubule profile. If the difference between these two distances was smaller than a single pixel size of the simulation (6 nm), then the R_i and R_o values of the corresponding simulated profile were retained for further analysis. The collected R_i and R_o values were averaged to find an average inner and outer radius of the DNA layer best fitted to experimental microtubule profiles. For example, the average R_i and R_o were 30.6 nm and 34.8 nm, respectively, for the experimental microtubule profile shown in **Supplementary Figure 2c**.

Code availability. iExM image simulator is contained in **Supplementary Software**.

Data availability statement. The data that support the findings of this study are available from the corresponding author upon request. Source data for **Figures 1** and **2** are available online

23. Klapoetke, N.C. *et al.* Independent optical excitation of distinct neural populations. *Nat. Methods* **11**, 338–346 (2014).
24. Chow, B.Y. *et al.* High-performance genetically targetable optical neural silencing by light-driven proton pumps. *Nature* **463**, 98–102 (2010).
25. Vaughan, J.C., Dempsey, G.T., Sun, E. & Zhuang, X. Phosphine quenching of cyanine dyes as a versatile tool for fluorescence microscopy. *J. Am. Chem. Soc.***135**, 1197–1200 (2013).
26. Legant, W.R. *et al.* High-density three-dimensional localization microscopy across large volumes. *Nat. Methods* **13**, 359–365 (2016).
27. Dell, R.B., Holleran, S. & Ramakrishnan, R. Sample size determination. *ILAR J.***43**, 207–213 (2002).

© 2017 Nature America, Inc., part of Springer Nature. All rights reserved.